wjert, 2024, Vol. 10 Issue 7, 12-39. Research Article ISSN 2454-695X

World Journal of Engineering Research and Technology
WJERT
www.wjert.org
SJIF Impact Factor: 7.029

ANALYSING THE STABILITY OF JEFFREY NANOFLUID'S MIXED CONVECTIVE FLOW OVER A POROUS MEDIUM

S. S. Saravanakumar[1]*, M. Sri Niveetha[2], M. Maheswari[3], P. S. Saritha[4] and S. Nagadeepa[5]

[1]Guest Lecturer, PG Research Department of Physics, Sethupathy Government Arts College, Ramanathapuram - 623502, Tamilnadu, India.

[2]Assistant Professor, Department of Physics, Sethu Institute of Technology, Kariyapatti, Tamilnadu, India.

[3]Head and Assistant Professor, Department of Physics, Noble College of Arts and Science for Women, Palavanatham, Virudhunagar District, Tamilnadu, India.

[4]Assistant Professor, Department of Physics, V V Vanniaperumal College for Women, Virudhunagar District, Tamilnadu, India.

[5]Assistant Professor, Department of Physics, Sethu Institute of Technology, Kariyapatti, Tamilnadu, India.

Article Received on 10/05/2024 **Article Revised on 30/05/2024** **Article Accepted on 20/06/2024**

***Corresponding Author**

S. S. Saravanakumar

Guest Lecturer, PG Research Department of Physics, Sethupathy Government Arts College, Ramanathapuram - 623502, Tamilnadu, India.

ABSTRACT

Using an unsteady Jeffrey-Darcy model, this work examines the stability of a mixed convective flow of a nanofluid across a horizontal porous layer. When evaluating the stability of a system, the base fluid is modeled as a Jeffrey fluid with scattered nanoparticles in a thermally equilibrium condition. This is done using linear stability theory. By employing Fourier decomposition to construct the stability equations as an eigenvalue issue, the higher orders Weighted Residual Galerkin Method (WRGM) is utilized to solve the problem and test the results analytically. The outcomes are displayed in terms of wave number, wave speed, and critical Darcy-Rayleigh number across nondimensional parameters. Furthermore, whereas the Vadasz number and the Jeffrey parameter have the opposite effect, nondimensional numbers like the thermal diffusivity ratio, the volume percentage of nanoparticles, and the horizontal pressure gradient have stabilizing effects. Furthermore, it has been noted that the stability zone shrinks

as the Jeffrey parameter increases. Even in the case of an infinite Vadasz number, the changing Jeffrey parameter alters the flow and hence nullifies the mathematical evidence of stability. The question of whether the basic flow is stable or unstable is answered by numerically addressing the eigenvalue problem across a finite range of the horizontal pressure gradient and Jeffrey parameter. These findings suggest that in order to increase the thermal efficiency of Jeffrey nanofluids, it is beneficial to estimate the volume percentage of nanoparticles that must be present in the base fluid. The effects of dimensionless parameters on physical systems are investigated using numerical and graphical studies, which shed light on the stability characteristics of the system under various circumstances.

KEYWORDS: *Jeffrey fluid, porous layer, nanofluid, instability, mixed convection, horizontal pressure gradient.*

INTRODUCTION

In the field of fluid dynamics, mixed convective flows of non-Newtonian fluids are an intricate and captivating subject of research. These fluids show behaviors that differ from the traditional Newtonian fluid model. Examples of these fluids are slurries, biological fluids, and polymer solutions. Both buoyancy forces from temperature gradients and outside pressures and forces affect the fluid motion in mixed convective flows. It is essential to comprehend the behavior of mixed convective non-Newtonian fluids in a variety of industrial processes, including oil recovery, food processing, and polymer processing. In order to understand the complex dynamics of these fluids and improve procedures for effectiveness and performance, researchers, engineers, and scientists frequently utilize sophisticated numerical models and experimental methods. Applications such as solar collectors, nuclear reactors, subterranean energy storage, and geothermal reservoirs all depend on an understanding of mixed convection in porous media.

Mixed convection in horizontal porous layers heated from below was studied by Prasad et al.[1], providing insight into the principles behind heat transmission in such systems. The significance of comprehending flow instabilities in porous media systems was underscored by Sphaier and Barletta's[2] investigation of unstable mixed convection in a heated horizontal porous channel. Through computer simulations, Ozgen and Varol[3] conducted a numerical investigation of mixed convection in a channel filled with a porous material, offering important insights into heat transmission processes in porous media. Our understanding of mixed convection in porous media and its implications for many technical and environmental

applications has improved as a result of these research taken together. Researchers may find a thorough reference covering a range of topics related to porous media and its applications in Vafai.[4] The potential of nanofluids to improve heat transmission in porous media was demonstrated by Kim and Vafai's[5] study on the use of nanofluids to buoyancy-driven heat transfer in porous enclosures. Understanding the impact of solid barriers on mixed convection in a lid-driven cavity filled with a fluid-saturated porous media was given by Abu-Nada and Chamkha.[6]

A thorough review of convection in porous media was given by Nield and Bejan[7], who emphasized the significance of this process for a range of engineering applications. The knowledge of transport processes in porous media was expanded by Ingham and Pop[8], who concentrated on theoretical and experimental issues. Using a porous medium model and the Navier slip boundary condition, Nield[9] made a significant contribution to the formulation of boundary conditions for porous media simulations. The impact of a horizontal pressure gradient and temperature difference for the Newtonian fluids on the start of Darcy-Bénard convection in thermally non-equilibrium conditions was the subject of a study by Postelnicu[10], which shed light on the interactions between pressure gradients and thermal non-equilibrium and clarified the mechanisms governing convective flow in porous media.

The phenomenon of free convection in Jeffrey nanofluids across porous media has been studied extensively. In a variety of applications, the study of Jeffrey nanofluid convection in porous media has improved heat transfer efficiency and energy conservation. These fluids perform better at heat transmission than traditional fluids because they make use of the special qualities of Jeffrey fluids as well as the heat-transfer capabilities of nanoparticles. They are especially helpful in applications like heat exchangers, cooling systems, and thermal management where effective heat transmission is essential. Jeffrey nanofluids can also lessen their negative effects on the environment, increase stability in high-temperature settings, and increase energy efficiency.[11] These characteristics highlight how exciting the topic of Jeffrey nanofluid convection research in porous media is, with enormous potential for real-world applications in a wide range of industries. As a result, the researchers were able to shed light on the thermal behavior of viscoelastic fluid flows in porous media and emphasize the significance of temperature differentials and pressure gradients in causing mixed convective instabilities.

In this work, we investigate the linear stability in mixed convection of Jeffrey's nanoporous fluid with the goal of improving our knowledge of the effects of porosity and nanoparticle properties on convection initiation. Since low-volume fraction and low-permeable porous channels are essential for controlling and optimizing convection, this discovery is especially pertinent to sectors like food processing and electronics cooling. We determine important parameters affecting convective motion using linear stability theory, as explained in the sections that follow.

Mathematical Formulation

The two-dimensional rectangular coordinate system (x, z) is chosen, where the x-axis is taken along the plates of the horizontal channel and the z-axis is perpendicularly upwards in which gravity $(\vec{g})$ is acting downwards. The plates at $z = d$ and $z = 0$ are maintained at dissimilar constant temperatures T_c and T_h respectively, with $T_h > T_c$ a porous matrix in between the plates. It is filled with -nanofluid which is heated from below and cooled from above as illustrated in **Figure 1**. The free and forced convection flow is due to the buoyant force with temperature difference $(\Delta T = T_h - T_c)$ and constant horizontal pressure gradient respectively leads to mixed convection flow. The following assumptions are made:

- A fully developed and non-quiescent base flow is assumed with an applied horizontal pressure gradient. Due to the low permeability of the porous channel, the unsteady Darcy model is adopted.
- The Boussinesq approximation $\rho = \rho_0(1 - \beta(T - T_c))$ is used such that the density varies only with temperature.
- The nanoparticle volume fraction is considered to be low and constant.[12]
- The study is restricted to linear stability along with normal mode analysis.
- The local thermal equilibrium between the fluid and solid phases holds in a porous medium.

Based on the aforementioned assumptions, the governing equations are formulated following the approach outlined by Yadav.[13]

$$\nabla . \vec{q} = 0 \tag{1}$$

$$\frac{\rho_{nf}}{\varepsilon}\frac{\partial \vec{q}}{\partial t} = -\nabla P - \rho_{nf}\beta_{nf}(\mathrm{T} - T_c)\vec{\mathrm{g}} - \frac{\mu_{nf}}{K(1+\lambda)}\vec{q} \tag{2}$$

$$\sigma\frac{\partial T}{\partial t}+\left(\vec{q}.\nabla\right)T=\frac{k_{nf}}{\left(\rho C_p\right)_{nf}}\nabla^2 T \tag{3}$$

The corresponding boundary conditions are given by

$$\vec{q}=0 \text{ at } z=0 \text{ and } z=\mathrm{d}, \tag{4}$$

$$T=T_h \text{ at } z=0 \text{ and } T=T_c \text{ at } z=d \tag{5}$$

Thermo-Physical Properties Of Nanofluids

The thermophysical properties of water-based nanofluid are used in the present study. The effective viscosity of the nanofluid, μ_{nf} is computed using the base fluid viscosity μ_{bf} and a diluted suspension of tiny sphere-shaped nanoparticles,

$$\mu_{nf}=\frac{\mu_{bf}}{\left(1-\phi\right)^{2.5}}, \tag{6}$$

Through experimental research using oil-water nanofluids at temperatures ranging from 20 to 50 degrees Celsius, the validation has been validated by.[14] The results of the experiments that followed are in[14] and show that it is entirely consistent. The[15] model is used to approximate the nanofluid's thermal conductivity. The model explains how the thermal conductivity of nanofluid rises with the aid of suspended nanoparticles and is provided by

$$k_{nf}=k_{bf}\left[\frac{\left(k_{np}+2k_{bf}\right)-2\phi\left(k_{bf}-k_{np}\right)}{\left(k_{np}+2k_{bf}\right)+\phi\left(k_{bf}-k_{np}\right)}\right] \tag{7}$$

At the reference temperature, the nanofluids effective density and heat capacitance are computed as[16,17] respectively as follows,

$$\rho_{nf}=\left(1-\phi\right)\rho_{bf}+\phi\rho_{np} \text{ and } \left(\rho C_p\right)_{nf}=\left(1-\phi\right)\left(\rho C_p\right)_{bf}+\phi\left(\rho C_p\right)_{np}, \tag{8}$$

Following are the formulas for nanofluids volumetric expansion coefficient and thermal diffusivity for nanofluids respectively,

$$\left(\rho\beta\right)_{nf}=\left(1-\phi\right)\rho_{bf}\beta_{bf}+\phi\rho_{np}\beta_{np} \text{ and } \alpha_{nf}=\frac{k_{nf}}{\left(\rho C_p\right)_{nf}}. \tag{9}$$

The characteristics of nano-fluids are explained using a single-phase jeffrey nano-fluid model, which is appropriate for low-volume concentrations of nanoparticles.

Table 1[18] displays the thermophysical characteristics of a number of nanoparticles at room temperature.

Non-Dimensional Governing Equations

The physical quantities of length, velocity, time, pressure, and temperature of nanofluid in the governing equations (1) – (5) are made non-dimensionalized using the scales $d, \frac{\varepsilon\alpha_{bf}}{d}, \frac{d^2}{\alpha_{bf}}, \frac{\varepsilon\mu_{nf}\alpha_{bf}}{K}$ and ΔT respectively and the following dimensionless governing equations in the cartesian coordinates are obtained by

$$\nabla.\vec{q} = 0 \tag{10}$$

$$\frac{1}{V_a}\frac{\partial\vec{q}}{\partial t} = -\nabla P + q_1 R_D T\hat{k} - \frac{\vec{q}}{(1+\Lambda)} \tag{11}$$

$$\frac{\partial T}{\partial t} + (\vec{q}.\nabla)T = \alpha_1\nabla^2 T \tag{12}$$

Where Λ is the nondimensional Jeffrey parameter, $R_D = \frac{\rho_{bf}\beta_{bf}K\,d\,g\,\Delta T}{\mu_{nf}\alpha_{bf}\varepsilon}$ is the Darcy-Rayleigh number, $q_1 = \frac{\rho_{nf}\beta_{nf}}{\rho_{bf}\beta_{bf}}$ is the nano-particle volume fraction ratio of nanofluid to base fluid, $\alpha_1 = \frac{\alpha_{nf}}{\alpha_{bf}}$ is the ratio of thermal diffusivity of nanofluid to base fluid, and $Va = \frac{\mu_{nf}\varepsilon d^2}{K\alpha_{nf}}$ is the Vadasz number.

The corresponding dimensionless boundary conditions are given by

$$\vec{q} = 0 \text{ at } z = 0,1,\ T = 1 \text{ at } z = 0 \text{ and } T = 0 \text{ at } z = 1 \tag{13}$$

Linear Stability Analysis

The linear stability analysis of mixed convection assumes a non-quiescent basic state of fluid flow, influenced by a constant horizontal pressure gradient as described in the following form,

$$\vec{q}_b = (u_b, w_b) = (\Pi, 0),\ P = P_b(z) \text{ and } T = T_b(z). \tag{14}$$

The corresponding basic state solutions are given by

$$u_b = \prod,\ T_b = 1 - z \text{ and } \mathrm{P}_b = \left(\frac{z^2}{2} - \mathrm{z}\right) q_1 R_D . \tag{15}$$

Further, we superimpose infinitesimally small perturbations on the basic state given in (15) in the form:

$$\vec{q} = \Pi i + \vec{q}',\ P = P_b(z) + P' \text{ and } T = T_b(z) + T' \tag{16}$$

The stability equations are derived by following a sequence of operations first we linearize equations (11) and (12) by substituting perturbed quantities given equation (16) then the pressure is eliminated by operating curl on the resultant equation ... and finally substituting stream function in the form $u = -\frac{\partial \psi}{\partial z}$ and $w = \frac{\partial \psi}{\partial x}$, we get

$$\left[\frac{1}{V_a}\frac{\partial}{\partial t} + \frac{1}{(1+\Lambda)}\right]\left(\frac{\partial^2 \psi}{\partial x^2} + \frac{\partial^2 \psi}{\partial z^2}\right) = q_1 R_D \frac{\partial T}{\partial x}, \tag{17}$$

$$\frac{\partial T}{\partial t} + \left\{\prod \frac{\partial T}{\partial x} - \frac{\partial \psi}{\partial x}\right\} = \alpha_1 \nabla^2 T . \tag{18}$$

At this moment for a better understanding of the impact of all parameters on the wave number and frequency of perturbations, the solution of equations (17) and (18) are expressed in the form of normal modes given by

$$(\psi, T) = (\Psi(z), \Theta(\mathrm{z}))e^{ia(x - \omega t)} \tag{19}$$

where a is the wavenumber and $\omega = \omega_r + i\omega_i$ is the complex wave speed. The growth rate ω_i marks the difference between stability $(\omega_i < 0)$ and instability $(\omega_i > 0)$. Substituting Eq. (19) in Eqs. (17) and (18), we obtain the following equations

$$\left[\frac{1}{(1+\Lambda)} - \frac{ia\omega}{V_a}\right](D^2 - a^2)\psi - iaq_1 R_D \Theta = 0, \tag{20}$$

$$ia\psi + \left[\alpha_1 (D^2 - a^2) + ia\omega - \Pi ia\right]\Theta = 0 . \tag{21}$$

The corresponding boundary conditions are given by

$$\psi = 0 = \Theta \text{ at } z = 0 \text{ and } \psi = 0 = \Theta \text{ at } z = 1 . \tag{22}$$

Growth Rate Analysis

The classical integral method, as described by Shankar and Shivakumara [19], is utilized to analyze the thermal instability in the limit as V_a approaches infinity. First, we operate $\left(D^2-a^2\right)$ on Eq. (21) to eliminate ψ and obtain the above equation for Θ in the form,

$$-a^2 q_1\left(1+\Lambda\right)R_D\Theta+\alpha_1\left(D^2-a^2\right)^2\Theta+ia\omega\left(D^2-a^2\right)\Theta-\Pi ia\left(D^2-a^2\right)\Theta=0$$

Multiply $\bar{\Theta}$ the complex conjugate form of Θ and integrate with respect to z over the limit 0 to 1, which yields

$$-a^2 q_1\left(1+\Lambda\right)R_D\int_0^1\Theta\bar{\Theta}\,dz+\alpha_1\int_0^1\left(D^2-a^2\right)^2\Theta\bar{\Theta}\,dz+ia\omega\int_0^1\left(D^2-a^2\right)\Theta\bar{\Theta}\,dz$$
$$-\Pi ia\int_0^1\left(D^2-a^2\right)\Theta\bar{\Theta}\,dz=0$$

We apply integration by parts to the above equation, we arrive at the following equation,

$$-a^2 q_1\left(1+\Lambda\right)R_D\int_0^1\left|\Theta\right|^2dz+\alpha_1\int_0^1\left(\left|\Theta''\right|^2+2a^2\left|\Theta'\right|^2+a^4\left|\Theta\right|^2\right)dz-ia\omega\int_0^1\left(\left|\Theta'\right|^2+a^2\left|\Theta\right|^2\right)dz$$
$$+\Pi ia\int_0^1\left(\left|\Theta'\right|^2+a^2\left|\Theta\right|^2\right)dz=0 \tag{23}$$

By evaluating the real part of Eq. (23), we obtain

$$\omega_i=\frac{-a^2 q_1\left(1+\Lambda\right)R_D\int_0^1\left|\Theta\right|^2dz+\alpha_1\int_0^1\left(\left|\Theta''\right|^2+2a^2\left|\Theta'\right|^2+a^4\left|\Theta\right|^2\right)dz}{-a\int_0^1\left(\left|\Theta'\right|^2+a^2\left|\Theta\right|^2\right)dz} \tag{24}$$

Thus, one may conclude that

(i) İf $a^2 q_1\left(1+\Lambda\right)R_D\int_0^1\left|\Theta\right|^2dz<\alpha_1\int_0^1\left(\left|\Theta''\right|^2+2a^2\left|\Theta'\right|^2+a^4\left|\Theta\right|^2\right)dz$ then $\omega_i<0$ indicating the system is stable, and

(ii) if $a^2 q_1\left(1+\Lambda\right)R_D\int_0^1\left|\Theta\right|^2dz>\alpha_1\int_0^1\left(\left|\Theta''\right|^2+2a^2\left|\Theta'\right|^2+a^4\left|\Theta\right|^2\right)dz$ then $\omega_i>0$ the system becomes unstable.

Method of Numerical Solutions

Equations (20) and (21) form a complex eigenvalue problem and are solved utilizing WRGM (Finlayson). In this method, the test (weighted) functions are the same as the base (trail)

functions. Accordingly, $\Psi(z)$ and $\Theta(z)$ are expanded in a finite series of basis functions in the form,

$$\Psi = \sum_{i=1}^{N} A_i \Psi_i(z), \text{ and } \Theta = \sum_{i=1}^{N} B_i \Theta_i(z) \tag{25}$$

Where A_i and B_i are constants while $\Psi_j(z)$ and $\Theta_j(z)$ are the basis functions and are generally chosen to satisfy the respective boundary conditions, respectively N represents the number of terms considered in the Galerkin expansion. The basis functions are described by the power series that adhere to the pertinent boundary conditions

$$\Psi_i = z^i - z^{i+1} = \Theta_i, \tag{26}$$

These series are substituted back into Equations (20) and (21) and the WRGM procedure of demanding that the residues be normal to the basis functions is applied by multiplying the resulting Eq. (20) by $\Psi_j(z)$ and Eq. (21) by $\Theta_j(z)$ integrating by parts with respect to z between $z = 0$ and $z = 1$, and the boundary conditions are used to obtain the following system of algebraic equations:

$$A_i E_{ji} + B_i F_{ji} = \omega A_i G_{ji} \tag{27}$$

$$A_i H_{ji} + B_i I_{ji} = \omega B_i J_{ji}, \tag{28}$$

The coefficients of E_{ji} and J_{ji} involve the inner products and are given by

$$\begin{aligned} E_{ji} &= \frac{1}{1+\Lambda}\left[\left\langle D\Psi_j\, D\Psi_i \right\rangle - a^2 \left\langle \Psi_j\, \Psi_i \right\rangle\right], \; F_{ji} = -iaq_1 R_D \left\langle \Psi_j\, \Theta_i \right\rangle, \\ \mathrm{G}_{ji} &= \frac{ia}{V_a}\left[\left\langle D\Psi_j\, D\Psi_i \right\rangle - a^2 \left\langle \Psi_j\, \Psi_i \right\rangle\right], \; H_{ji} = ia\left\langle \Theta_j \Psi_i \right\rangle, \\ \mathrm{I}_{ji} &= -\left[\alpha_1 \left\langle D\Theta_j\, D\Theta_i \right\rangle + \left(\alpha_1 a^2 + ia\Pi\right)\left\langle \Theta_j\, \Theta_i \right\rangle\right], \; J_{ji} = -ia\left\langle \Theta_j \Theta_i \right\rangle. \end{aligned} \tag{29}$$

Where the inner product is defined by $\langle ... \rangle = \int_0^1 (...)\, dz$ equations (27) and (28) can be written in the matrix form as

$$AX = \omega BX \tag{30}$$

Where

$$A = \begin{bmatrix} E_{ji} & F_{ji} \\ H_{ji} & I_{ji} \end{bmatrix}, B = \begin{bmatrix} G_{ji} & 0 \\ 0 & J_{ji} \end{bmatrix} \text{ and } X = \begin{bmatrix} A_i \\ B_i \end{bmatrix}$$

Equation (30) forms a generalized eigenvalue problem in which that A and B are $2N \times 2N$ order complex matrices, X is the eigenvector and $\omega = \omega_r + i\omega_i$ is the complex eigenvalue.

The integral occurring in the coefficients of E_{ji} and J_{ji} are analytically evaluated to avoid errors during the numerical integration. The main stages of the numerical procedure involved in solving Eq. (30) are as follows

i) Among the $2N$ eigenvalues, we identify the most growing or the least decaying mode having the largest imaginary part of the eigenvalue ω and call that mode simply the most growing mode.

ii) The largest value of ω_i is now forced to zero by varying R_D for a fixed value of wave number a and other governing parameters.

The computational software program MATHEMATICA 11.3 (Wolfram Research) is used to provide an ideal platform for the execution of both stages and the following built-in functions are used

$$Max[Im[Eigenvalues[A,B]]] = EV(say) and\ Find\ Root[EV[R_D, a] == 0].$$

RESULTS AND DISCUSSIONS

This paper uses a generalized eigenvalue problem to analyse and computationally examine the mixed convective instability of Jeffrey nanofluid flow over a horizontal porous layer. The findings gained by adapting both single-term and higher-order Galerkin approaches are reported by evaluating the Galerkin expansion's convergence process while adding more words.

Table (2-4) illustrates the WGRM's convergence process for a range of governing parameter values. It is observed that taking into account 10 terms in WGRM allows for the convergence of the critical Darcy-Rayleigh number, the associated critical wave number, and the critical frequency. We have carefully investigated and verified our numerical method's validity and convergence. The results are computed under the limiting situation in order to validate the numerical approach used, and it is shown that there is great agreement.

A glance at **Tables (2-4)** shows that there is not much deviation in the values of critical stability parameters between the second ($N = 2$) and higher order ($N = 10$) (WGRM). Thus it is intuitive to look for the analytical solution for the eigenvalue problem with $\Psi = A sin \pi z$

and $\Theta = Bsin\pi z$ as basis functions for the solutions of equations (20) and (21). By substituting these into Equations (20) and (21), we can express them in the matrix form as follows

$$\begin{bmatrix} \left(\frac{1}{1+\Lambda} - \frac{ia\omega}{V_a}\right)\delta^2 & iaq_1R_D \\ ia & -\alpha_1\delta^2 - i\Pi a + ia\omega \end{bmatrix} \begin{bmatrix} \Psi \\ \Theta \end{bmatrix} = \begin{bmatrix} 0 \\ 0 \end{bmatrix} \tag{31}$$

where, $\delta^2 = a^2 + \pi^2$.

Equation (31) represents a homogeneous system and for a non-trivial solution, we should have

$$\begin{vmatrix} \left(\frac{1}{1+\Lambda} - \frac{ia\omega}{V_a}\right)\delta^2 & iaq_1R_D \\ ia & -\alpha_1\delta^2 - i\Pi a + ia\omega \end{vmatrix} = 0 \tag{32}$$

Solving this determinant for R_D, we get

$$R_D = \frac{\delta^2\left\{iV_a + a(1+\Lambda)\omega\right\}\left[-i\delta^2\alpha_1 + (\Pi - \omega)a\right]}{a^2q_1V_a(1+\Lambda)} \tag{33}$$

After rearranging this expression, it is represented in a complex form as follows,

$$R_D = \Delta_1 + i\omega\,\Delta_2 \tag{34}$$

Where

$$\Delta_1 = \frac{\delta^2\left[\pi^2V_a\alpha_1 + a^2\left\{V_a\alpha_1 - (1+\Lambda)(\Pi - \omega_i)\omega_i\right\}\right]}{a^2q_1V_a(1+\Lambda)}, \tag{35}$$

$$\Delta_2 = \frac{a\delta^2\left[V_a(\Pi - \omega_i) + \delta^2\alpha_1(1+\Lambda)\omega_i\right]}{a^2q_1V_a(1+\Lambda)}. \tag{36}$$

Since R_D is a physical quantity, we take $\Delta_2 = 0\ (\omega_i \neq 0)$ in Eq. (34) and this gives a dispersion relation of the form:

$$b_1\omega_i + b_0 = 0. \tag{37}$$

Where,

$b_1 = aV_a\,\delta^2\,\Pi$,

$b_0 = -aV_a\,\delta^2 + \alpha_1\delta^4\left(1+\Lambda\right).$

Equation (37) reveals that for an appropriate combination of the governing parameters Π, q_1, α_1, Λ, and V_a. The minimum value of R_D and ω_i over the wave number a is numerically found for several values of controlling parameters. The results so obtained are also given in **Table (2-4)** in the last row and the results are in excellent agreement with those computed numerically from WGRM.

The equation (34) suggests that the preferred mode is always oscillatory. Thus, for a Newtonian fluid, $q_1 = 1$ and $\alpha_1 = 1$ then equation (33) reduces to

$$R_D = \frac{\delta^2\left\{-iV_a + a\left(1+\Lambda\right)\omega\right\}\left\{i\,\delta^2 + a\left(\omega-\Pi\right)\right\}}{a^2V_a\left(1+\Lambda\right)} \tag{38}$$

The above expression in the equation (38), with $\Pi = 0$ and $\omega = 0$, subsequently reducing to

$$R_D = \frac{\delta^4}{a^2\left(1+\Lambda\right)} \tag{39}$$

This expression matches with[13] and represents the onset of stationary convection limiting the case to LTE. The above expression is in the equation (39) with $\Lambda = 0$ which coincides with Horton and Rogers, Lapwood's Problem.

$$R_{Dc} = \frac{\delta_c^{\,4}}{a_c^{\,2}}. \tag{40}$$

Analysis of the Growth Rate

The critical wave number and growth rate ω_i are plotted in **Figures 2-5** for various values of R_D, Λ, Π and different nanoparticles. The growth rate helps us comprehend the onset of instability in the $\left(a, \omega_i\right)$ plane. The sign of ω_i determines the stability of the system: if $\omega_i < 0$, the system is stable, and if $\omega_i > 0$, it is unstable. **Figure 2** shows a plot for TiO_2 ($\alpha_1 = 10,\ q_1 = 0.97$) nanoparticles with $\Pi = 2,\ \Lambda = 0.3,$ and $V_a = 1$ for various values of R_D. We observe that the curve starts from a negative value and remains negative for lower values of R_D signifying that the base flow is always linearly stable, and for higher values of R_D the sign of ω_i changes from negative to positive indicating the possibility of the flow becoming

unstable. In **Figure 3**, for $R_D = 250$, ω_i is positive for $\Lambda = 0.9$ and 0.7, indicating the occurrence of transition from stability to instability for all considered values, whereas for $\Lambda = 0.3$ and 0.5, it is stable. In **Figure 4**, by varying Π with $R_D = 316$, while keeping other parameters fixed as mentioned above, it is observed that the fluid flow for $\Pi = 2,4,6$ enters the positive regime of ω_i indicating the onset of instability, while for $\Pi = 8$ the curve passes through the maximum in the negative region of ω_i ensuring the stability of the flow. A significant change in the curve's behavior is observed when considering different nanoparticles (**Figure 5**). Specifically, TiO_2 and Al_2O_3 particles show instability, while CuO particles remain stable for the considered parametric values.

Neutral Stability Curves

The neutral stability curves presented in **Figures (6-9)** depict the relationship between the Darcy-Rayleigh number (R_D) and a wave number (a) in (a, R_D)-plane by considering various physical parameters, including the Jeffrey parameter, horizontal pressure gradient, Vadasz number, thermal diffusivity ratio, and different nanoparticle ratios. These curves exhibit a uni-modal nature similar to those observed in classical Darcy–Bénard problems, indicating the occurrence of a single mode of convection. A deeper look at the graphs reveals a few crucial findings. **Figure 6** illustrates how the stability zone decreases as the Jeffrey parameter increases. As the Vadasz number increased, similar behavior was observed (**Figure 9**). This behavior can be explained by the higher fluid viscosity that results from higher Vadasz numbers and Jeffrey parameters, which obstruct fluid mobility and cause the system to become unstable. On the other hand, the stability area expands when the horizontal pressure gradient rises (**Figure 7**). This is because the fluid is subjected to a greater driving force, which improves fluid motion and encourages stability.

Moreover, **Figure 8** shows that the stability zone decreases with a drop in the Darcy-Rayleigh number brought on by nanoparticle ratios. This is explained by variations in convective heat transfer and fluid flow patterns brought about by the kind of nanoparticles altering the thermal conductivity and viscosity of the nanofluid. Furthermore, the decrease in the stability zone suggests that a rise in the Jeffrey parameter and nanoparticle ratios destabilizes the system.

Additionally, **Figure 8** demonstrates the comparative stability of water-CuO, water- Al_2O_3 and water TiO_2 nanofluids. It suggests that CuO dispersed in water exhibits more excellent stability than water- Al_2O_3 and water TiO_2 nanofluid, primarily due to the differences in thermal conductivity and thermal sensitivity of the nanoparticles. Specifically, CuO nanoparticles contribute to enhanced heat transfer and stability, whereas water TiO_2 and Al_2O_3 nanofluids display instability owing to its higher thermal sensitivity, which can lead to thermal fluctuations and convective instability. In summary, the findings from the neutral stability curves provide valuable insights into the complex interplay between various parameters and their effects on the stability of Jeffrey nanofluid flow through porous media. These insights contribute to a deeper understanding of the underlying mechanisms governing convective behavior and have implications for designing and optimizing thermal management systems in various engineering applications.

Critical Curves

The behavior of R_{Dc}, a_c, and ω_{ic} as functions of Π is elucidated in **Figures (10-12)** for different values of the Jeffrey parameter Λ, specifically Λ = 0.3, Λ = 0.5, and Λ = 0.7. **Figure (10)** shows that the critical Darcy-Rayleigh number R_{Dc} remains invariant for small values of Π, indicating a stable regime. However, beyond $\Pi > 2$, Π starts to influence R_{Dc}, increasing its increase. Additionally, an increase in the Jeffrey parameter Λ is noted to decrease the critical Darcy-Rayleigh number R_{Dc}, thereby advancing the onset of convection. **Figure (11)** shows that the critical wave number a_c decreases with rising values of Π, consequently diminishing the size of the convection cells. Conversely, in **Figure (12)**, the necessary frequency ω_{ic} decreases with increasing Λ values, indicating a stabilizing effect, while it increases with rising Π, suggesting enhanced oscillatory behavior.

Similarly, the behavior of R_{Dc}, a_c, and ω_{ic} as functions of Π are explored in **Figures (13-15)** for different values of the Vadasz number V_a, specifically V_a = 1, V_a = 10, and V_a = 20. In **Figure (13)**, it is observed that in the critical Darcy-Rayleigh number R_{Dc}, the effect of small Π values are negligible but start to increase beyond Π = 1, signifying the influence of Π on R_{Dc} and subsequent destabilization. Moreover, an increase in V_a is observed to expand the stability region, thus delaying the onset of convection. **Figure (14)** shows that the critical wave number a_c decreases with an increase in V_a and Π values, leading to a reduction in the

size of convection cells. Finally, in **Figure (15)**, the critical frequency ω_{ic} is seen to increase with increasing Π values, while it increases with increasing V_a, reflecting the system's response to changes in flow parameters.

Further, the plots of R_{Dc}, a_c, and ω_{ic} as functions of Λ are illustrated in **Figures. (16-18)** for different values of V_a = 1, 10, and 20. **Figure (16)** reveals a linear decrease in the critical Darcy-Rayleigh number R_{Dc} with increasing Λ. Hence, it destabilizes the system. Also, a similar trend is observed with an increase in V_a. In **Figure (17)**, an increase in Λ and V_a is seen to increase and decrease a_c, respectively, leading to changes in the size of convection cells. Finally, in **Figure (18)**, the values of ω_{ic} are observed to increase with increasing V_a values. In contrast, an opposite effect could be seen with an increase in Λ, indicating the system's response to variations in flow parameters.

Analysis of the data presented in **Table 5** reveals a consistent trend: as the Jeffrey parameter increases, there is a notable decrease in the critical Darcy Rayleigh number across all three types of nanoparticles under examination. This suggests that higher Jeffrey parameters enhance these nanofluids' convective stability. Specifically, when focusing on CuO nanoparticles, it becomes apparent that they exhibit a maximal critical Darcy Rayleigh number compared to the other nanoparticle types. This maximal value indicates that CuO nanoparticles possess superior thermal stability relative to their counterparts. On the other hand, the wave frequency demonstrates a contrasting behavior. Across all nanoparticle types, there is a discernible decrease in wave frequency. Notably, Al_2O_3 nanoparticles exhibit the highest frequency among the studied particles. Drawing insights from these observations, it can be inferred that the onset of convection varies across the different nanoparticles. For Al_2O_3 nanoparticles, the onset of convection appears to be at an intermediate stage. In contrast, for TiO_2 nanoparticles, convection onset occurs more rapidly. Interestingly, for CuO nanoparticles, the onset of convection unfolds much more gradually compared to the other nanoparticle types. These nuanced distinctions in convection onset further underscore the complex interplay between nanoparticle characteristics and fluid dynamics.

Table 1: Thermo-physical properties of nanoparticles.

Physical properties	CuO	Al_2O_3	TiO_2
Cp(J/KgK)	531.80	765.00	686.20
ρ (Kg/m^3)	6320.00	3970.00	4250.00
k(W/mK)	76.50	40.00	8.95
α × 10^7 (m^2/s)	227.60	131.70	307.00
β × 10^5 (1/K)	1.80	0.85	0.90

Table 2: Convergence of the Wrgm for different values of Π with $\varphi = 0.025$ for TiO_2 nanoparticles.

$\alpha_1 = 10,\ q_1 = 0.97,\ \Lambda = 0.5,\ V_a = 2$									
	$\Pi = 2$	$\Pi = 5$	$\Pi = 10$						
N	R_{Dc}	a_c	ω_{ic}	R_{Dc}	a_c	ω_{ic}	R_{Dc}	a_c	ω_{ic}
3	293.5132	3.2659	0.0124	294.9386	3.2658	0.0310	300.0294	3.2655	0.0621
4	270.3464	3.1342	0.0134	271.7703	3.1341	0.0337	276.8556	3.1337	0.0674
5	271.5368	3.1412	0.0134	272.9608	3.1410	0.0335	278.0465	3.1407	0.0671
6	271.6027	3.1415	0.0134	273.0267	3.1414	0.0335	278.1124	3.1410	0.0671
7	271.6013	3.1415	0.0134	273.0253	3.1414	0.0335	278.1109	3.1410	0.0671
8	271.6005	3.1415	0.0134	273.0245	3.1414	0.0335	278.1102	3.1410	0.0671
9	271.6005	3.1415	0.0134	273.0245	3.1414	0.0335	278.1102	3.1410	0.0671
10	271.6005	3.1415	0.0134	273.0245	3.1414	0.0335	278.1102	3.1410	0.0671
One term	271.6005	3.1415	0.0134	273.0245	3.1414	0.0335	278.1102	3.1410	0.0671

Table 3: Convergence of the Wrgm for different values Of Π with $\varphi = 0.075$ for Ti_{o2} nanoparticles.

$\alpha_1 = 9.9075,\ q_1 = 0.9387,\ \Lambda = 0.5,\ V_a = 2$									
	$\Pi = 2$			$\Pi = 5$			$\Pi = 10$		
N	R_{Dc}	a_c	ω_{ic}	R_{Dc}	a_c	ω_{ic}	R_{Dc}	a_c	ω_{ic}
4	276.7819	3.1342	0.0136	278.2668	3.1341	0.0340	283.5701	3.1337	0.0680
5	278.0006	3.1412	0.0135	279.4857	3.1410	0.0338	284.7893	3.1406	0.0677
6	278.0681	3.1415	0.0135	279.5531	3.1414	0.0338	284.8568	3.1410	0.0677
7	278.0666	3.1415	0.0135	279.5517	3.1414	0.0338	284.8553	3.1410	0.0677
8	278.0658	3.1415	0.0135	279.5509	3.1414	0.0338	284.8546	3.1410	0.0677
9	278.0659	3.1415	0.0135	279.5509	3.1414	0.0338	284.8546	3.1410	0.0677
10	278.0659	3.1415	0.0135	279.5509	3.1414	0.0338	284.8546	3.1410	0.0677
One term	278.0659	3.1415	0.0135	279.5509	3.1414	0.0338	284.8546	3.1410	0.0677

Table 4: Convergence of the Wrgm for different values of Π with $\varphi = 0.1$ for Tio_2 nanoparticles.

$\alpha_1 = 9.8113,\ q_1 = 0.9182,\ \Lambda = 0.5,\ V_a = 1$									
	$\Pi = 2$			$\Pi = 5$			$\Pi = 10$		
N	R_{Dc}	a_c	ω_{ic}	R_{Dc}	a_c	ω_{ic}	R_{Dc}	a_c	ω_{ic}
5	271.0724	3.1411	0.0069	283.2749	3.1406	0.0137	288.5694	3.1390	0.0375
6	281.2463	3.1416	0.0069	283.4489	3.1410	0.0137	288.7436	3.1394	0.0375
7	281.2426	3.1416	0.0069	283.4451	3.1410	0.0137	288.7398	3.1394	0.0375
8	281.4914	3.1416	0.0069	283.0340	3.1415	0.0171	288.5467	3.1413	0.0343
9	281.4914	3.1416	0.0069	283.0340	3.1415	0.0171	288.5467	3.1413	0.0343
10	281.4914	3.1416	0.0069	283.0340	3.1415	0.0171	288.5467	3.1413	0.0343
One term	281.4914	3.1416	0.0069	283.0340	3.1415	0.0171	288.5467	3.1413	0.0343

Table 5: Critical values of R_{Dc}, a_c and ω_{ic} for different combinations of nanoparticles and Jeffrey parameter.

	CuO ($V_a = 2,\ \Pi = 5$) $\alpha_1 = 73.2993, q_1 = 0.9657$ ($\varphi = 0.075$)			Al_2O_3 ($V_a = 2,\ \Pi = 5$) $\alpha_1 = 39.2427, q_1 = 0.9371$ ($\varphi = 0.075$)			TiO_2 ($V_a = 2,\ \Pi = 5$) $\alpha_1 = 9.9075, q_1 = 0.9387$ ($\varphi = 0.075$)		
Λ	R_{Dc}	a_c	ω_{ic}	R_{Dc}	a_c	ω_{ic}	R_{Dc}	a_c	ω_{ic}
0	2996.8773	3.14159	0.00690	1653.90400	3.14158	0.012876	419.30855	3.14139	0.050619
0.3	2305.2904	3.14159	0.00531	1272.23450	3.14159	0.009910	322.55454	3.14143	0.039028
0.5	1997.9184	3.14159	0.00460	1102.60350	3.14159	0.008591	279.55094	3.14145	0.033859
0.7	1762.8692	3.14159	0.00406	972.88558	3.14159	0.007582	246.66508	3.14147	0.029899
0.9	1577.3041	3.14159	0.00363	870.47668	3.14159	0.006785	220.70210	3.14148	0.026769

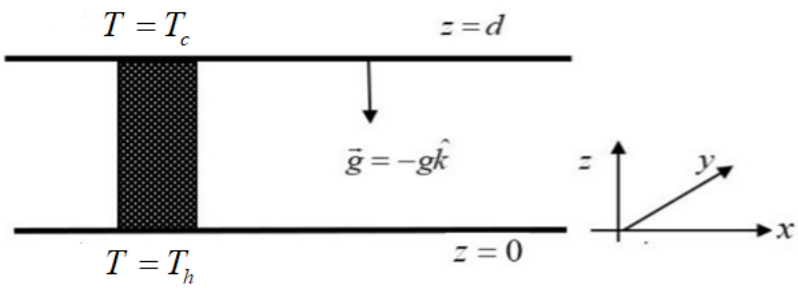

Figure 1: Physical Configuration.

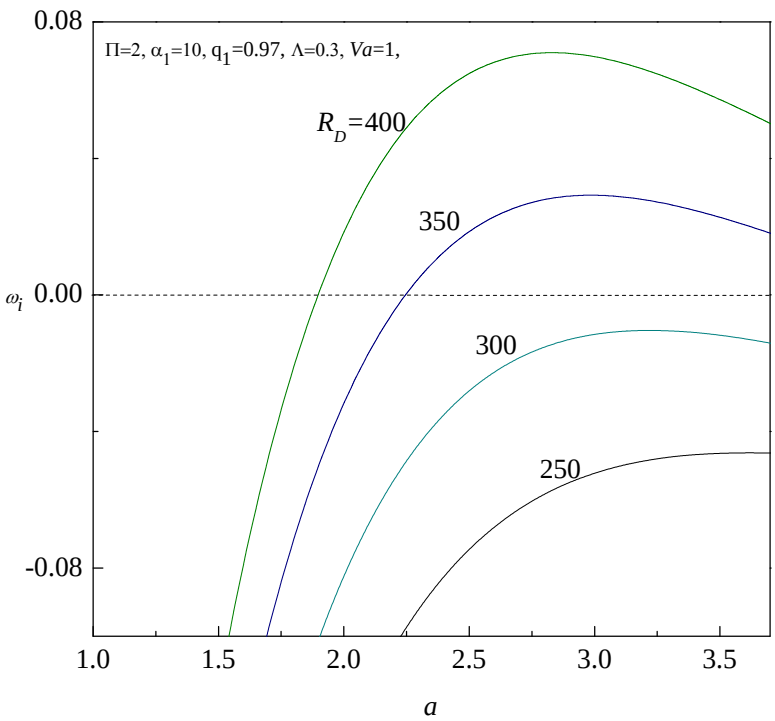

Figure 2: Growth rate ω_i versus wavenumber a for different values of R_D.

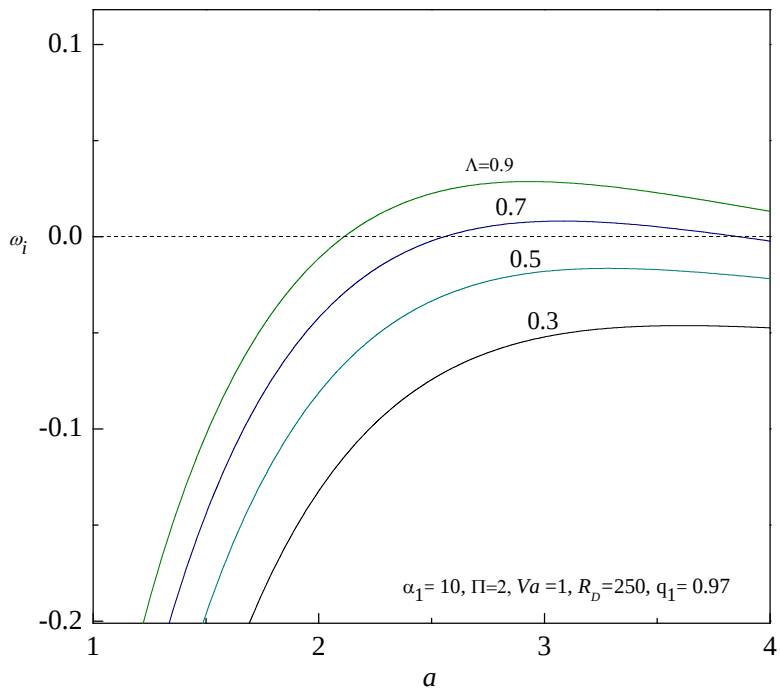

Figure 3: Growth rate ω_i versus wavenumber a for different values of Λ.

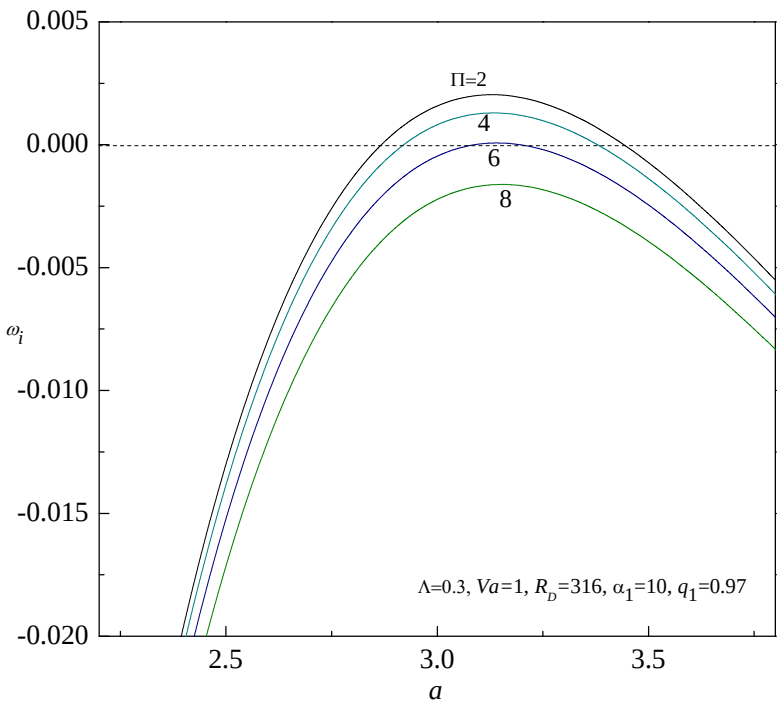

Figure 4: Growth rate ω_i versus wavenumber a for different values of Π.

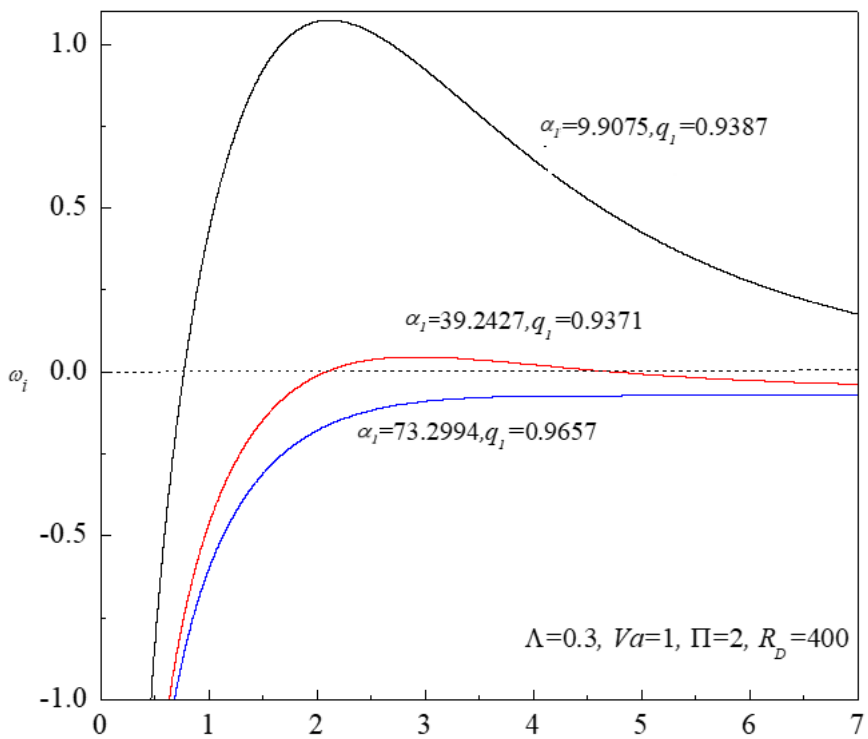

Figure 5: A significant change in the curve's behavior is observed when considering different nanoparticles.

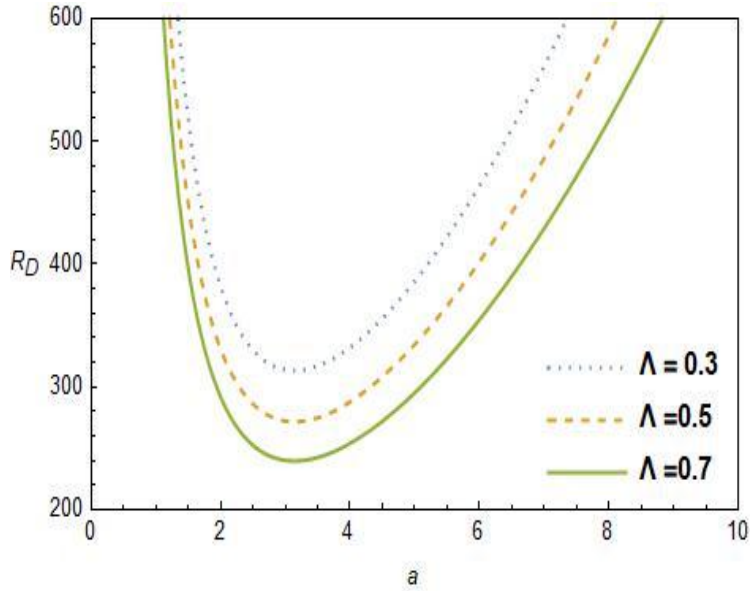

Figure 6: Neutral Stability curves for different values of Λ **with** $\alpha_1 = 10$, $q_1 = 0.97$, $\Pi = 2$ **and** $V_a = 1$.

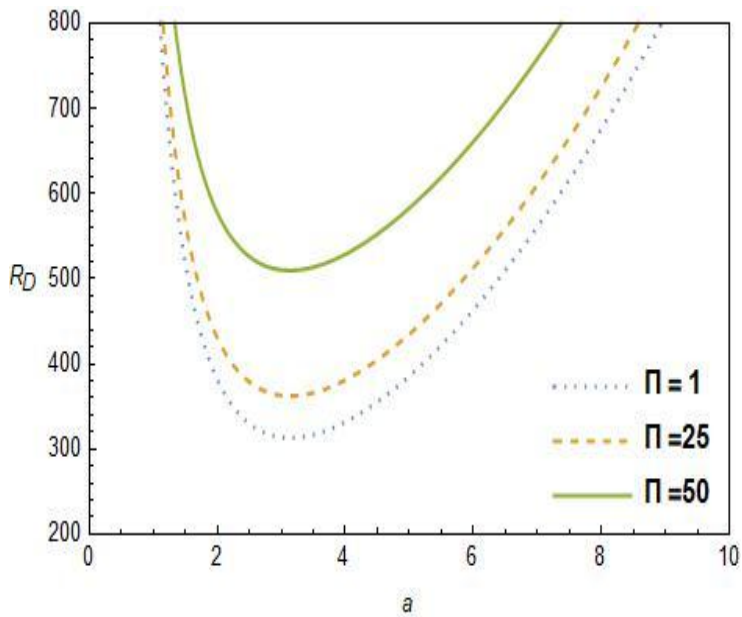

Figure 7: Neutral Stability curves for different values of Π **with** $\alpha_1 = 10, q_1 = 0.97$, $V_a = 1$ **and** $\Lambda = 0.3$.

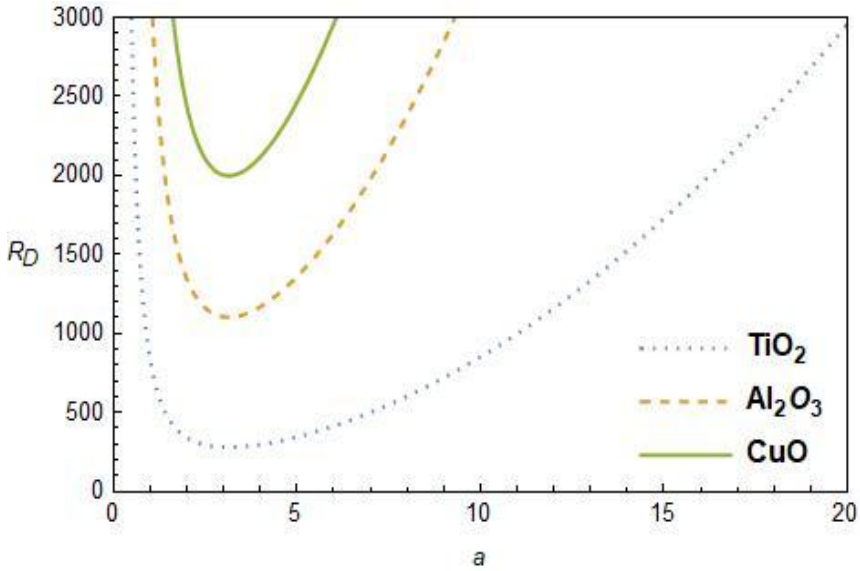

Figure 8: Neutral Stability curves for different nanoparticles with, $\phi = 0.075$**,** $\Pi = 5, V_a = 2$ **and** $\Lambda = 0.5$**.**

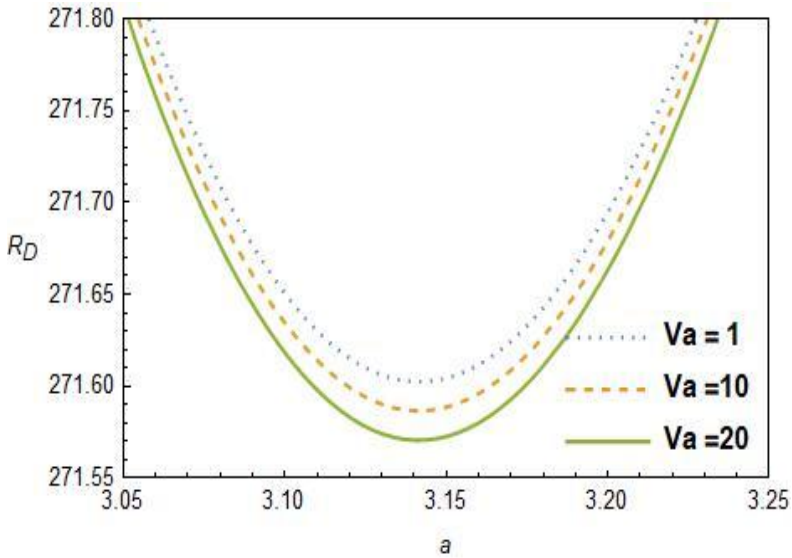

Figure 9: Neutral Stability curves for different values of V_a **with** $\alpha_1 = 10$**,** $q_1 = 0.97, \Pi = 2$ **and** $\Lambda = 0.5$**.**

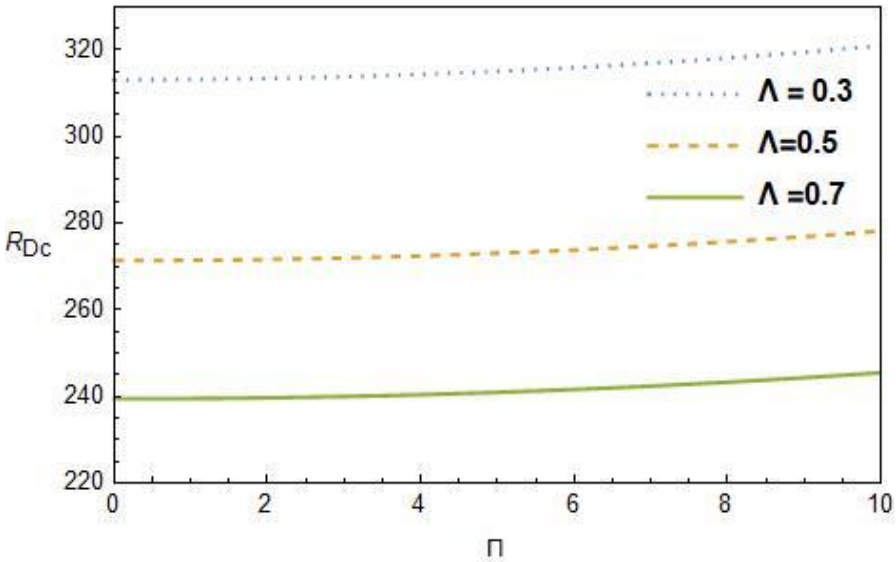

Figure 10: Critical curves of Darcy-Rayleigh number as a function of Π for different values of Λ with $\alpha_1 = 10$, $q_1 = 0.97$, and $V_a = 1$.

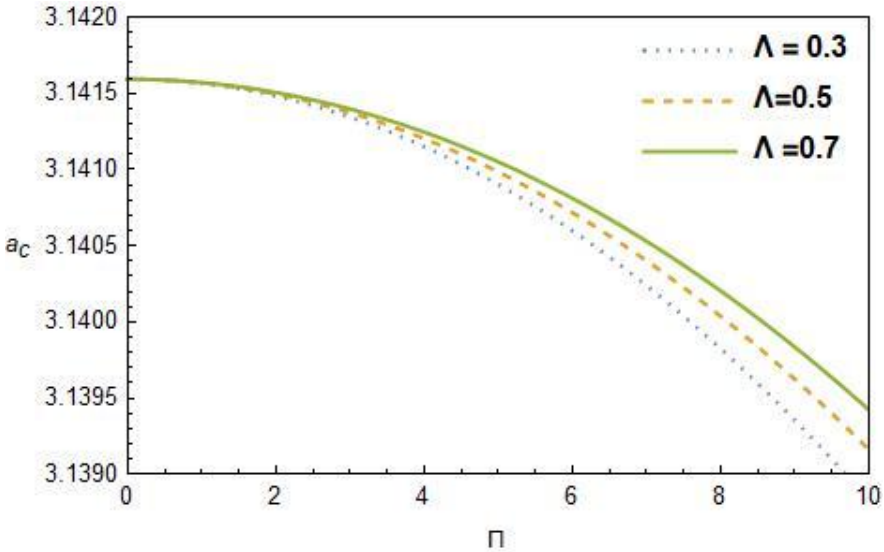

Figure 11: Critical curves of wave number as a function of Π for different values of Λ with $\alpha_1 = 10$, $q_1 = 0.97$ and $V_a = 10$.

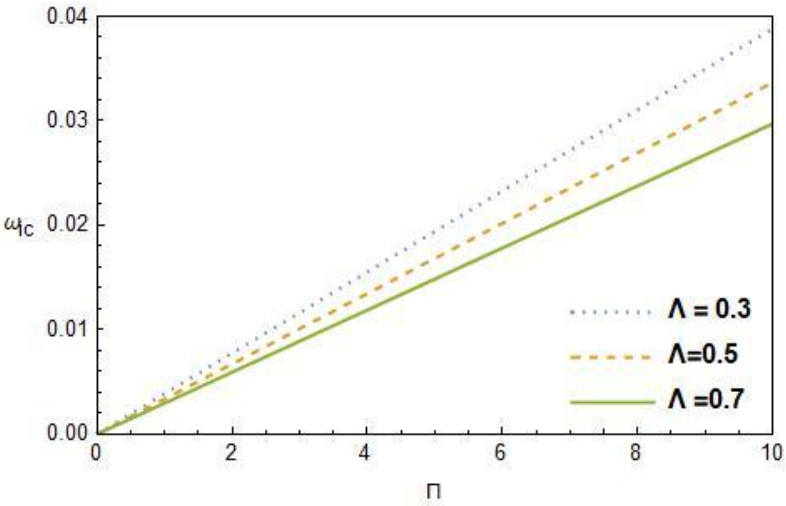

Figure 12: Critical curves of wave frequency as a function of Π for different values of Λ with $\alpha_1 = 10$, $q_1 = 0.97$ and $V_a = 1$.

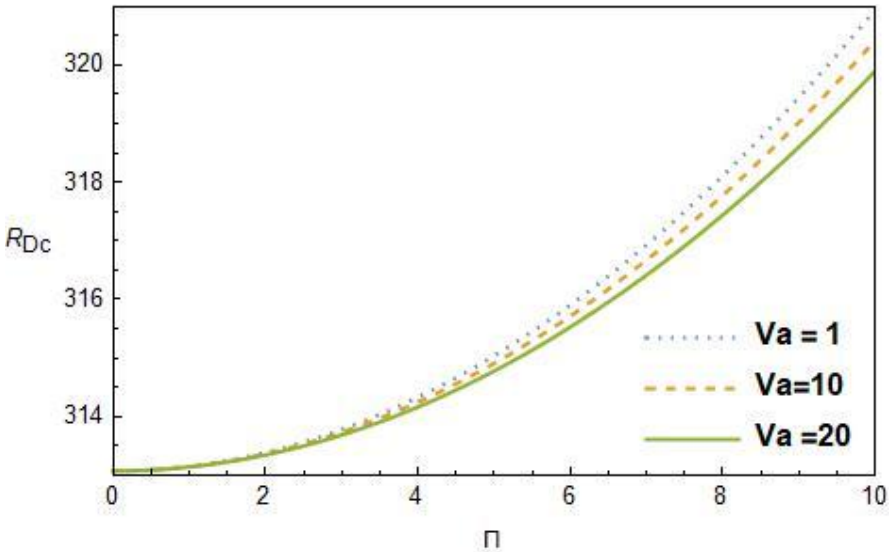

Figure 13: Critical curves of R_{Dc} Vs Π for different values of V_a with $\alpha_1 = 10, q_1 = 0.97$ and $\Lambda = 0.3$.

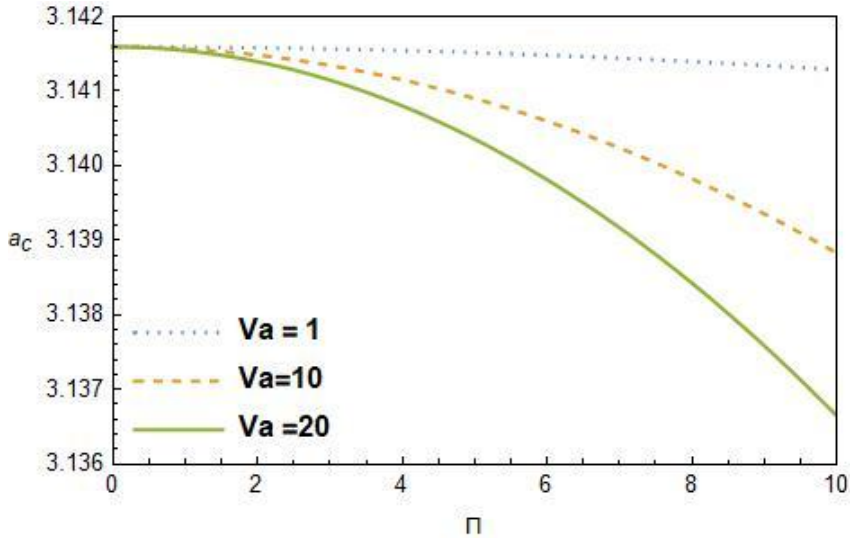

Figure 14: Critical curves of a_c Vs Π for different values of V_a with $\alpha_1 = 10, q_1 = 0.97$ and $\Lambda = 0.3$.

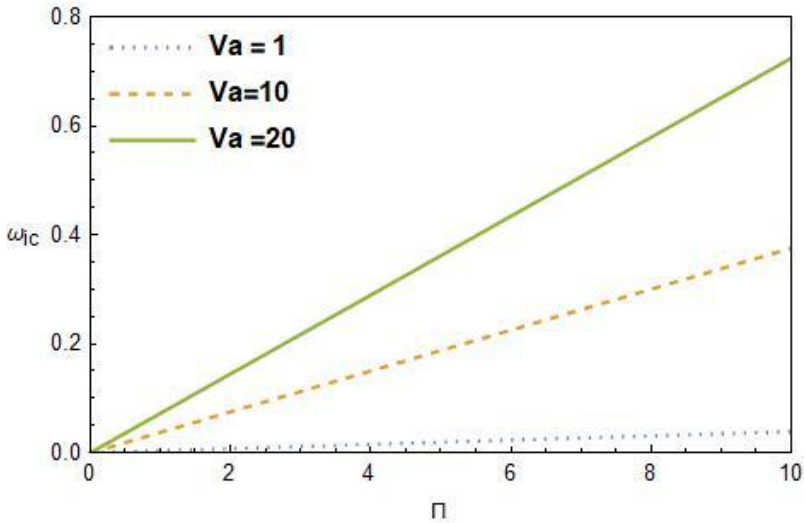

Figure 15: Critical curves of ω_{ic} Vs Π for different values of V_a with $\alpha_1 = 10, q_1 = 0.97$ and $\Lambda = 0.3$.

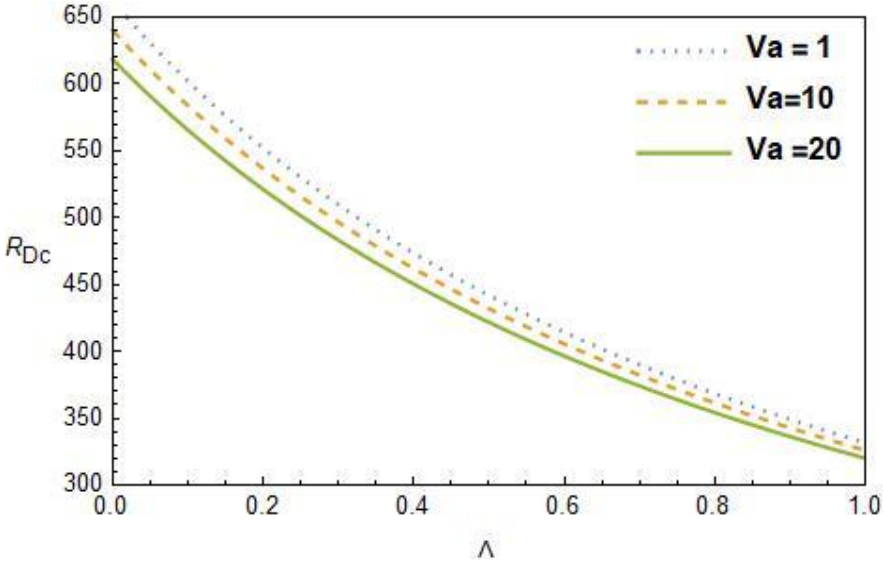

Figure 16: Critical curves of R_{Dc} Vs Λ for different values of V_a with $\alpha_1 = 10, q_1 = 0.97$ and $\Pi = 50$.

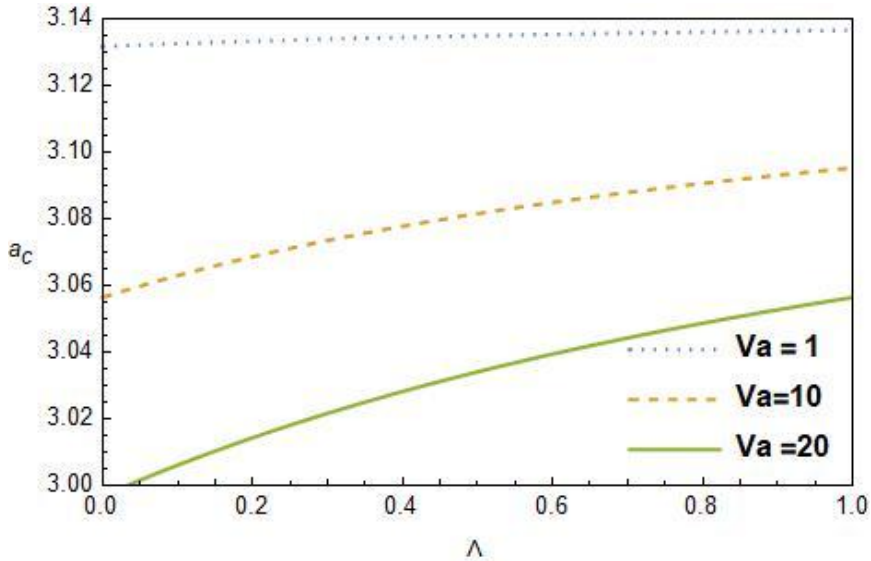

Figure 17: Critical curves of a_c Vs Λ for different values of V_a with $\Pi = 5, V_a = 2$ and $\Pi = 50$.

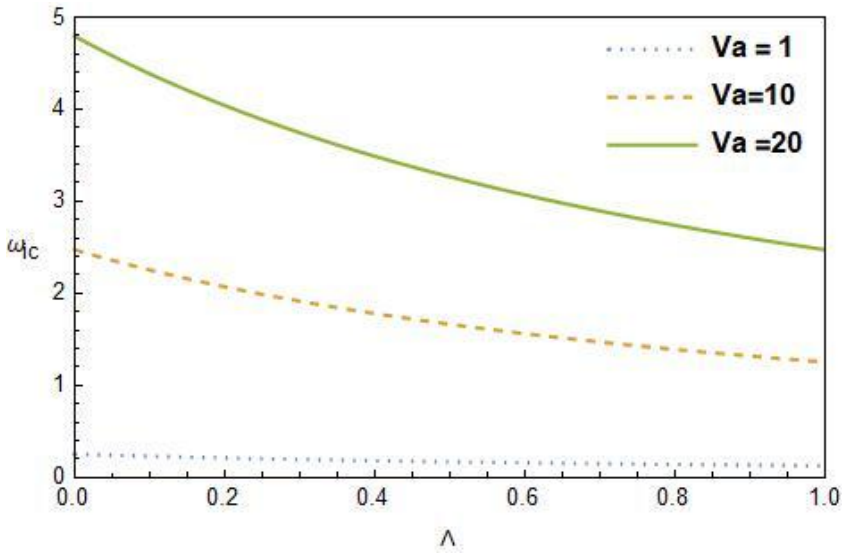

Figure 18: Critical curves of ω_{ic} Vs. Λ for different values of V_a with $\Pi = 5, V_a = 2$ and $\Pi = 50$.

CONCLUSIONS

In this study, we performed a thorough stability analysis of mixed convective flow with a volume fraction of Jeffrey nanofluid in a porous layer, using both numerical and analytical methods. The study utilized the unsteady Jeffrey-Darcy model, which includes the Jeffrey parameter to address retardation or relaxation effects. This model is particularly well-suited for situations involving low-volume fraction Jeffrey nanoparticles and porous layers with low permeability. Specifically, we utilized the Weighted Residual Galerkin Method (WRGM) for numerical analysis and the single-term Galerkin method for analytical investigation. It is shown that the results are in good agreement with N=8. Also, the growth rate of perturbations is numerically computed over a broad spectrum of governing parameters, revealing a notable change in the growth rate behavior for TiO_2 and Al_2O_3 particles, exhibiting instability, while CuO particles remain stable within the considered parametric range. Some of the important results of this analysis can be outlined as follows

- The neutral stability curves exhibit a single minimum, and we observe that the instability region diminishes with increasing nanoparticle volume fraction in the base fluid. This phenomenon suggests that higher volume fractions result in amplified resistance to flow.
- Increasing Π leads to an expansion of the stability region, indicating a stabilizing effect. Conversely, an increasing value of the Jeffrey parameter Λ results in a contraction of the stability region for all nanoparticles, implying a destabilizing influence.

- Increasing the Vadasz number is to decrease the Darcy-Rayleigh number hence advances the onset of convection.
- An increase in the Jeffrey parameter Λ tends to decrease the critical values of R_{Dc} and ω_{ic}, accelerating the initiation of convective activity. However, a_c exhibits a reverse trend, decreasing a_c value with an increase of Λ for all nanofluids, indicating a stabilizing effect on convective cell size.
- We observe that the Jeffrey parameter Λ can act as both a stabilizer and a destabilizer, depending on its combination with other parameters, highlighting its versatile role in influencing convective stability. These conclusions provide valuable insights into the complex interplay of parameters affecting the stability of mixed convective flow in Jeffrey nanofluids through porous media, contributing to a deeper understanding of thermal transport phenomena in such systems.
- The critical Darcy-Rayleigh number for various nanoparticles exhibits an inequality of the form $\left(R_{Dc}\right)_{CuO} > \left(R_{Dc}\right)_{Al_2O_3} > \left(R_{Dc}\right)_{TiO_2}$.

REFERENCES

1. V. Prasad, F. C. Lai, and F. A. Kulacki, "Mixed convection in horizontal porous layers heated from below,", 1988; 395-402.
2. L. A. Sphaier and A. Barletta, "Unstable mixed convection in a heated horizontal porous channel," International Journal of Thermal Sciences, 2014; 78: 77-89.
3. F. Ozgen and Y. Varol, "Numerical study of mixed convection in a channel filled with a porous medium," Applied Sciences, 2019; 9(2): 211.
4. K. Vafai, "Handbook of porous media," CRC press, 2005.
5. Y. Kim and K. Vafai, "Buoyancy-driven heat transfer enhancement in a two-dimensional porous enclosure utilizing nanofluids," International Journal of Heat and Mass Transfer, 2006; 49(13-14): 2402-2414.
6. E. Abu-Nada and A. J. Chamkha, "Mixed convection flow in a lid-driven cavity filled with a fluid-saturated porous medium: Effect of a conducting vertical solid plate on the left wall," International Journal of Heat and Mass Transfer, 2007; 50(3-4) 727-735.
7. D. A. Nield and A. Bejan, "Convection in porous media," Springer Science & Business Media, 2006.
8. D. B. Ingham and I. Pop, "Transport phenomena in porous media III," Elsevier, 2013.

9. D. A. Nield, "A note on a porous medium model with the Navier slip boundary condition," International Journal of Heat and Mass Transfer, 2013; 62: 287-291.
10. A. Postelnicu, "The effect of a horizontal pressure gradient on the onset of a Darcy-Bénard convection in thermal non-equilibrium conditions," International Journal of Heat and Mass Transfer, Jan., 2010; 53(1–3): 68–75. doi: 10.1016/j.ijheatmasstransfer.2009.10.006.
11. Pallavi, G., Hemanthkumar, C., Shivakumara, I.S., Rushikumar, B. Oscillatory Darcy-Bénard-Poiseuille Mixed Convection in An Oldroyd-B Fluid-Saturated Porous Layer. In: Rushi Kumar, B., Sivaraj, R., Prakash, J. (eds) Advances in Fluid Dynamics. Lecture Notes in Mechanical Engineering. Springer, Singapore, 2021. https://doi.org/10.1007/978-981-15-4308-1_63.
12. N. Singh, M. K. Khandelwal, "Linear stability perspective on mixed convection flow of nanofluids in a differentially heated vertical channel," International Communications in Heat and Mass Transfer, 2022; 134. doi: 10.1016/j.icheatmasstransfer.2022.105989.
13. D. Yadav, "Influence of anisotropy on the Jeffrey fluid convection in a horizontal rotary porous layer," Heat Transfer, vol. 50, no. (5): 4595–4606. doi: 10.1002/htj.22090.
14. Y. Xuan, Q. Li, "Investigation on convective heat transfer and flow features of nanofluids," Journal of Heat Transfer, vol. 125, pp. 151–155, 2003, doi: 10.1115/1.1532008.
15. J. C. Maxwell, A Treatise on Electricity and Magnetism, Cambridge University Press, 2010.
16. K. Khanafer, K. Vafai, M. Lightstone, "Buoyancy-driven heat transfer enhancement in a two-dimensional enclosure utilizing nanofluids," International Journal of Heat and Mass Transfer, vol. 46, pp. 3639–3653, 2003.
17. Y. Xuan, W. Roetzel, "Conceptions for heat transfer correlation of nanofluids," International Journal of Heat and Mass Transfer, 2000.
18. N. Singh and M. K. Khandelwal, “Linear stability perspective on mixed convection flow of nanofluids in a differentially heated vertical channel,” International Communications in Heat and Mass Transfer, vol. 134, May 2022, doi: 10.1016/j.icheatmasstransfer.2022.105989.
19. Shankar, B. M., and I. S. Shivakumara. "Gill's stability problem may be unstable with horizontal heterogeneity in permeability." Journal of Fluid Mechanics 943,(2022: A20.